Orientation selection in photosynthetic PS I multilayers: structural investigation of the charge separated state $P_{700}^{+\cdot}$ $A_1^{-\cdot}$ by high-field/high-frequency time-resolved EPR at 3.4 T/95 GHz

M. Fuhs[a,*], A. Schnegg[a], T. Prisner[c], I. Köhne[a], J. Hanley[b,1], A.W. Rutherford[b], K. Möbius[a]

[a] *Institut für Experimentalphysik, Freie Universität Berlin, Arnimallee 14, D-14195 Berlin, Germany*
[b] *Service de Bioénergétique, CNRS, URA 2096, CEA Saclay, F-91191 Gif-sur-Yvette, France*
[c] *Institut für Physikalische und Theoretische Chemie, Johann-Wolfgang-Goethe, Universität, Marie Curie Str. 11, D-60439, Frankfurt, Germany*

Abstract

The radical-pair state of the primary electron donor and the secondary electron acceptor ($P_{700}^{+\cdot}$ $A_1^{-\cdot}$) of the photosynthetic reaction center (RC) photosystem I (PS I) of *Synechocystis* PCC 6803 was studied by time-resolved electron paramagnetic resonance (TREPR) at high field/high frequency (3.4 T/95 GHz) using orientation selection in multilayers. The goal of the present article is to work out the basis for future studies, in which the improved resolution of such multilayers may be used to detect mutation-induced structural changes of PS I in membrane preparations. This approach is particularly interesting for systems that cannot be prepared as single crystals. However, in order to use such multilayers for structural investigations of protein complexes, it is necessary to know their orientation distribution. PS I was chosen as a test example because the wild type was recently crystallized and its X-ray structure determined to 2.5 Å resolution [Nature 411 (2001) 909]. On the basis of our experimental results we determined the orientation distribution. Furthermore, a simulation model for the general case in which the orientation distribution is not axially symmetric about the C_2 symmetry axis of the RC is developed and discussed. Spectra simulations show that changes in the TREPR spectra of PS I are much more significant for these oriented multilayers than for disordered samples. In this way the use of oriented multilayers, in conjunction with multifrequency TREPR measurements on oriented as well as on disordered samples, is a promising approach for studies of structural changes of PS I systems that are induced by point mutations.
© 2002 Elsevier Science B.V. All rights reserved.

Keywords: Photosystem I; Orientation selection; Multilayer; Time-resolved high-field EPR; Radical pair

1. Introduction

In recent years, multifrequency time-resolved electron paramagnetic resonance (TREPR) on photosynthetic reaction centers (RCs) of various organisms has been successfully used to obtain structural information on the cofactors involved in charge separated radical-pair states which are created after light excitation [1–5]. In this way, TREPR has contributed to the elucidation of the structure–function relationship of the highly efficient electron-transfer reac-

tions in these photosystems. In plant photosystem I (PS I), after photo-excitation of the primary electron donor, P_{700}, which is a chlorophyll *a* dimer, an electron is transferred via the primary electron acceptor, A_0, to the secondary acceptor, A_1, which is a phylloquinone (for reviews, see Refs. [6,7]). At room temperature, the electron is further transferred to a series of iron–sulfur clusters. Below 200 K, in a significant fraction of RCs the electron transfer to the iron–sulfur centers is blocked and the charge-separated state, $P_{700}^{+\cdot} A_1^{-\cdot}$, has a life time of about 10^{-4} s, before it decays by direct recombination to the round state, $P_{700}A_1$ [6]. With pulsed and continuous wave (cw) TREPR on $P_{700}^{+\cdot} A_1^{-\cdot}$ at different magnetic fields/microwave frequencies, it has been possible to determine accurate values of distance and relative orientation of $P_{700}^{+\cdot}$ and $A_1^{-\cdot}$ [8–10]. These results, together with addi-

* Corresponding author. Tel.: +49-30-838-53587; fax: +49-30-838-56046.

E-mail address: michael.fuhs@physik.fu-berlin.de (M. Fuhs).

[1] Present address: Gen Odyssee S.A., Parc d'Affaires Technopolis, 3 avenue du Canada, Batiment Alpha-BP 810, Les Ulis 91974 Courtaboef cedex, France.

tional EPR data from single crystals of deuterated RCs [11] and with X-ray structure data at 4-Å resolution [12,13] (now resolved even to 2.5 Å [14,15]), led to a structural model for P_{700}^{+} $A_1^{-\cdot}$ published recently [11].

On the other hand, the effect of structural parameters on TREPR line shapes of disordered samples in frozen solution is obscured by unresolved hyperfine interactions and, moreover, by overlapping resonance lines. Both effects contribute to inhomogeneous line broadening. Consequently, enhanced resolution can be obtained by using higher and higher magnetic fields and microwave frequencies and, of course, by using single crystals, which contain the RCs with specific orientations. Both strategies have technical limitations and, in particular, the production of single crystals is difficult, time-consuming and even impossible for many protein systems. Therefore, we have used RC multilayers that provide 1D orientation selection. In these multilayers, the RCs are oriented with their C_2 symmetry axis perpendicular to the layer surface [16]. This allows one to select this unique orientation and, by turning the multilayer in the magnetic field, to obtain specific rotation patterns with 1D orientation selection. 1D oriented multilayers have been used before in combination with high-field/high-frequency EPR to study doublet radicals of cofactors of PS I [17] and PS II [18]. For 0.34 T/9.5 GHz EPR (X-band), multilayers with orientation selection have been used for many years (e.g. [16]), more recently also for studies of spin-echo decays from radical-pair states of PS I and PS II [19]. Furthermore, in contrast to disordered samples, multilayers provide additional information on the orientation of cofactors with respect to the membrane [17]. Naturally, the ordering in multilayers is not perfect and, consequently, additional complications for the data analysis emerge from the uncertainty of orientation distribution parameters.

Here we present the first high-field/high-frequency TREPR measurements at 3.4 T/95 GHz (W-band) on oriented multilayers of PS I from *Synechocystis* PCC 6803. The measurements on such samples are a real challenge to spectrometer sensitivity. We had to develop two novel plane-concave Fabry–Pérot resonators, one with the plane mirror oriented parallel and the other with the plane mirror oriented perpendicular to the external magnetic field. For the data analysis in terms of structural information, we developed a spectra-simulation model for the 1D orientation selection which includes also anisotropy of the orientation distributions. Consequently, the distributions are not axially symmetric with respect to the C_2 symmetry axis of the RCs. Our W-band spectra can be simulated well with the set of parameters recently published [11]. Additionally, we determine the orientation-distribution parameters of the multilayer sample in order to use them in future projects on other systems, e.g., mutant PS I preparations [20–23]. On this basis we compare the effect of structural parameters on TREPR spectra of disordered samples and of oriented multilayers, considering the uncertainties of orientation distribution parameters and phase errors.

2. Experimental

2.1. Sample preparation

The PS I membranes were grown from wild-type *Synechocys-tis* PCC 6803, isolated and prepared as described in Ref. [17]. Membrane fragments and PS I trimers were spread onto thin mylar sheets and dried at 4 °C at a humidity of 80% over 2–4 days [17]. The multilayers were treated with sodium dithionite in order to reduce the $P_{700}^{+\cdot}$ prior to cooling. The multilayers were kept under argon at −15 °C in the dark. For measurements in the Fabry–Pérot resonators, the mylar sheets were cut into pieces of 1 cm^2 and fixed on the plane mirrors with a small amount of vacuum grease.

2.2. W-band TREPR spectrometer

The TREPR experiments were performed in direct-detection mode, i.e., without magnetic field modulation. Positive signals, therefore, indicate absorption (*a*), negative signals emission (*e*) of microwave radiation. For each magnetic field point, the signal was averaged over the indicated integration window after each laser flash, and the average signal of a similar integration window before the laser flash was subtracted in order to retain only light-generated signals. For a typical spectrum, 50 averages were taken for each magnetic field position. The laboratory-built time-resolved 95-GHz high-field EPR spectrometer is described elsewhere [24]. The time resolution is about 10 ns. The microwave power for the TREPR experiments was about 0.25 mW at the Fabry–Pérot resonator. The samples were photo-excited by using a frequency doubled Nd:YAG laser (532 nm) with a repetition rate of 10 Hz. The measuring temperature was 160 K. Phase adjustment and field calibration were performed before running the TREPR experiments using the cw EPR signal of a Mn^{2+}/MgO standard sample [25]. From experience we estimate that the field-calibration error due to the delay between the recording of cw and TREPR spectra is about 0.5 mT.

2.3. Plane-concave Fabry–Pérot resonators

In order to obtain good orientation selection with multilayers on plane surfaces, we have developed two novel plane concave Fabry–Pérot resonators with the external magnetic field either parallel or perpendicular to the plane mirror (Fig. 1). Basically, the experiment could be also performed using cylindrical single-mode cavities [24] with the advantage that one could rotate the multilayers and measure all intermediate orientations of the multilayer orthogonal with respect to the magnetic field. From our preliminary experiments using a cylindrical cavity, it is our experience, however, that it is difficult to introduce the multilayer into the tiny W-band cavity and, because for sufficient sensitivity one has to stack several small multi-
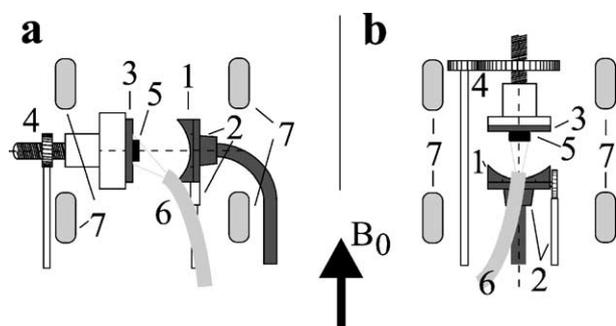
Fig. 1. Plane–concave Fabry–Pérot resonators with light excitation for W-band EPR (3.4 T/95 GHz) with (a) B_0 parallel and (b) perpendicular to the plane mirror. The resonators are operated in the modes $TEM_{005-007}$. 1: concave mirror. 2: coupling mechanism. 3: plane mirror. 4: resonance frequency adjustment. 5: sample. 6: light fiber for optical excitation for TREPR experiments. 7: magnetic field modulation coils for cw experiments.

layer strips of 0.8-mm width, orientation selection gets less well defined.

The Fabry–Pérot resonators are matched to the wave guide by moving a thin dielectric plate (macor) partially over the iris of the concave mirror [25]. The plane mirror can be shifted to adjust the resonance frequency. Both adjustments, microwave matching and frequency tuning, have to be repeated when the temperature has changed. The microwave beam-waist diameter on the plane mirror, on which the multilayer sample is attached, is about 4 mm and, correspondingly, the size of the multilayers for optimal sensitivity should be about 12.5 mm^2. With the 0.25-mW microwave power at the Fabry–Pérot resonator, the maximum B_1 field at the center of the sample is about 0.06 mT. The cw sensitivity was determined to be about 4×10^9 spins/ $(mT\sqrt{Hz})$. The light excitation in Fabry–Pérot resonators is more difficult than in cylindrical cavities, because it is not possible to use angles of incidence of the light fiber smaller than 60° with respect to the mirror normal. The aperture of the light beam emerging from the fiber is about 15° and, therefore, great care must be taken to focus the spot on the central region of the mirror. This is particularly difficult when one has to readjust the dimensions of the resonator after having changed the temperature. The spot on the plane mirrors was determined by measuring the strong triplet TREPR signal of small photo-excited pentacene crystals which, step by step, were fixed at different positions on the mirrors.

3. Spectra simulations

3.1. Simulation of radical-pair spectra

The simulations were performed using the correlated-coupled-radical-pair (CCRP) model described in the literature [1,2,26–29]. The two unpaired electrons located on P_{700}^+ and A_1^- are subject, in addition to the external Zeeman field, to local magnetic fields described by the anisotropic G and hyperfine structure (hfs) tensors of the two radicals. Furthermore, the two electron spins are coupled by their dipolar interaction, which is described by an axial zero-field-splitting tensor with coupling parameter D. The exchange interaction J_{ex} in the system is negligible due to the relatively large distance of the radical-pair partners in PS I (25.4±0.3 Å [8,10]). Because the interactions are anisotropic, the transient radical-pair spectra are very sensitive to distance and relative orientation of the radical-pair partners. The radical pairs are created in the singlet state after photo-excitation and subsequent singlet electron transfer. The transient radical-pair systems are spin polarized by singlet-triplet ST_0 mixing and, in the CCRP model, for each orientation of the radical pair with respect to the Zeeman field one observes four EPR resonance lines. They are all equal in absolute intensity, but two of them are in absorption and two in emission. Because relaxation effects, which would alter the line shape, are rather slow at the sample temperature (160 K), it is justified to integrate the TREPR spectra for about 1 ms after the laser pulse and to use the static CCRP model for the theoretical analysis. The hfs has to be included explicitly for spectra simulations at 0.34 mT X-band EPR [30]. At 3.4 mT W-band EPR, however, the hfs leads mainly to inhomogeneous line broadening. Thus, it is sufficient to convolute the spectra simulations, which had been performed without taking hfs into account, with a Gaussian line shape of 0.7 mT FWHM width.

We want to emphasize that the assumptions of the CCRP model made for the PS I systems studied in this article may not hold for all radical pair systems of interest. For instance, in systems which are affected by relaxation effects on a short time scale, the absolute intensity of the four resonance transitions at one molecular orientation will not remain equal (see Ref. [31]). However, by using the appropriate theory, the orientation selection approach can be used for these systems in the same way as for the PS I RCs. The theory developed in the next sections remains valid.

3.2. Simulations of 1D oriented spectra

The PS I RCs are oriented with their C_2 symmetry axis parallel to the normal n of the multilayer [16]. Concerning the rotation about the C_2 axis, the orientation of PS I is random and, therefore, the multilayers provide only a 1D orientation selection, in contrast to 3D orientation selection in single crystals. Furthermore, one has to consider two additional sources of disorder: (i) disorder of the C_2 axis with respect to n because of incomplete order in the multilayer itself, (ii) disorder of the cofactors within the RCs. The second type of disorder is negligible, as was shown by studies both on disordered samples and single crystals. In both cases the experimental results could be well described with fixed relative orientations of the cofactors in PS I [11]. Therefore, only the first type of disorder has to be considered

for the spectra simulations. Consequently, one has to determine the probability $P(o)$ with which the RC has the orientation o.

The simulation of the 1D orientation selection in multilayers has been described in depth [18] for the calculation of EPR spectra of doublet-state cofactors in PS II. In order to describe an arbitrary orientation distribution of 3D objects, it is necessary to use distributions of two of the three Euler angles rather than of one angle. This is true not only for 3D, but also for 1D orientation selection (in contrast to the case of magnetic-field-induced orientation selection [32]). Fig. 2a shows schematically the calculation procedure according to Ref. [18], when applied to radical-pair spectra. In the laboratory (LAB) coordinate system, B_0 is directed along z_{LAB}. The intermediate reference system (IRF) is turned by θ, i.e., $<(B_0 z_{IRF}) = \theta$. The direction of the projection of B_0 in the $x_{IRF} y_{IRF}$ plane is random over which one integrates during the calculation procedure. The orientation distribution is included as a Gaussian distribution of the second as well as of the third Euler angle of the individual cofactors. In this way, one takes into account possible anisotropies in the orientation distribution, for example when it is not axially symmetric in terms of rotations about C_2. However, when the anisotropy is included as a Gaussian distribution of Euler angles, $P_1(\gamma_2)$ and $P_2(\gamma_3)$ in the case of A_1^- in PS I, implicitly one has chosen already a particular direction of the anisotropy. A general description would require a more complicated function for $P(\gamma_2, \gamma_3) \neq P_1(\gamma_2) P_2(\gamma_3)$. This becomes evident when one has to consider not only one but three different reference systems, as is the case for radical-pair spectra. Using the known relative orientations of the coordinate systems of P_{700}^+, A_1^- and of the ZFS tensor, the spectra simulations depend on which of the three sets of Euler angles has been chosen for the description of the orientation distribution.

Therefore, we have developed a model which is closer to the experimental conditions. It is shown schematically in Fig. 2b and c. In the LAB coordinate system with the Zeeman field directed along z_{LAB}, it is sufficient to use one angle, θ, to describe the position of the sample mirror in the magnet. The orientation of one individual RC with respect to the sample mirror is given by the three Euler angles, α_1, α_2 and α_3 (membrane system, MEM). For $\theta = 0$, because of the axial symmetry of the experimental set-up, α_1 has no physical meaning. Within the RC the location of the cofactors P_{700}^+ and A_1^- is given by additional sets of Euler angles, β_i and γ_i, as indicated in Fig. 2. Furthermore, the orientation of the ZFS tensor is given by Euler angles ζ_i. Because the ZFS tensor is axial, the third Euler angle ζ_3 is redundant. Because the main orientation effect orients the C_2 axes of the RCs along the multilayer normal n in this extended model the orientation distribution P is, to first approximation, a Gaussian function of the angle α_2, the angle of the sample-mirror normal with respect to the C_2 axis. Because the RCs and membrane fragments, which have to orient with respect to each other, are not axially
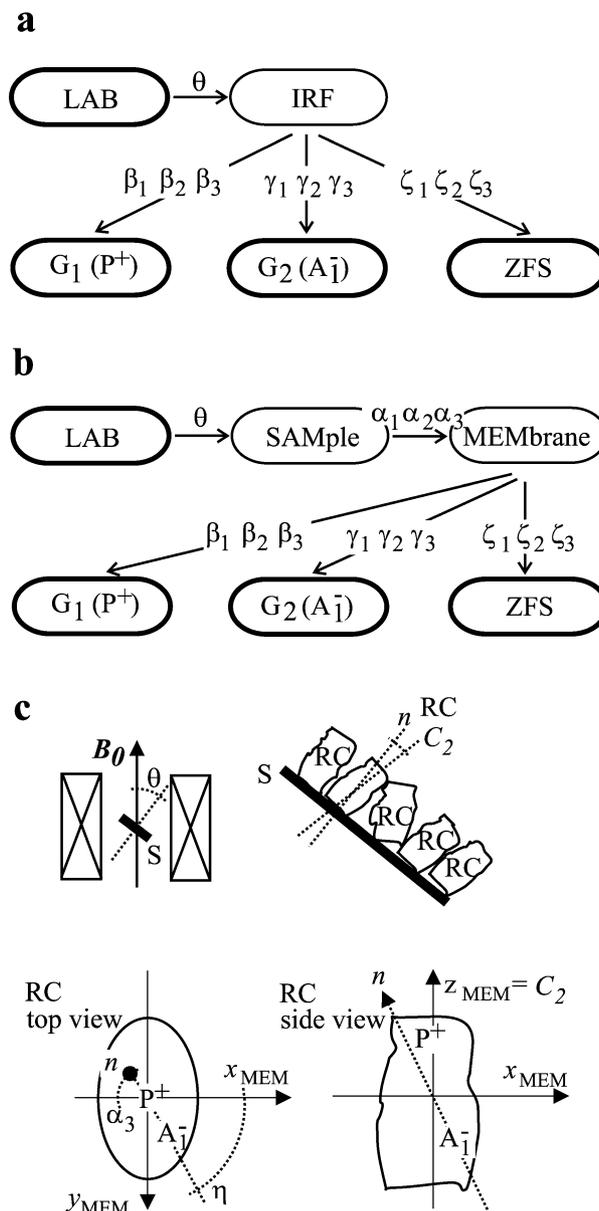

Fig. 2. Description of 1D orientation selection. Angles are defined as Euler angles for rotations about z with first angle, about y' with a second angle and about z'' with a third angle. (a) Model of axes systems adapted from Ref. [18]. It was used to calculate EPR spectra of doublet radicals in PS II in 1D oriented membranes. (b) Model used in this work. (c) Further illustration of this model. The sample mirror (S) is rotated by θ about an axis perpendicular to B_0 (top left). The orientation of individual RCs with respect to the sample mirror is given by the angles α_1, α_2 and α_3. Their orientation deviates from perfect orientation selection ($n \parallel C_2$) according to Eqs. (1a)–(1b) (top right). Top and side views of a reaction center which is not perfectly aligned are shown at the bottom. η is defined by convention (Eqs. (2a)–(2c)). For more explanations, see text.

symmetric, it is reasonable at this point to include possible deviations from axial symmetry of the orientation distribution. We use an elliptical function. Consequently, the width of the orientation distribution in α_2 depends also on α_3, which is the angle of the projection of n in the $x_{MEM} y_{MEM}$ membrane plane with respect to x_{MEM}. With the (FWHM/

$\sqrt{2\ln 2}$) widths, $\varDelta_x$ and $\varDelta_y$ for $\alpha_3=0°$ and $\alpha_3=90°$, respectively, we use for the orientation distribution

$$P(\alpha_2, \alpha_3) = \exp[-2\alpha_2^2/\varDelta^2(\alpha_3)] \tag{1a}$$

$$\varDelta(\alpha_3) = \sqrt{\varDelta_x^2\cos^2(\alpha_3) + \varDelta_y^2\sin^2(\alpha_3)}. \tag{1b}$$

In this model for describing the nonaxial orientation distribution it is necessary to consider, as an additional parameter, the angle η (see Fig. 2c). Here η contains information about the orientation of the cofactors in the $x_{MEM}y_{MEM}$ membrane plane with respect to the main axis of the elliptical orientation distribution. Consequently, η is given by the angle of the projection of the dipolar axis in the $x_{MEM}y_{MEM}$ plane with respect to x_{MEM}. Angle η is implicitly contained in the first Euler angles for the cofactors which, therefore, are redefined as

$$\beta_1 = \beta_1^0 + \eta \tag{2a}$$

$$\gamma_1 = \gamma_1^0 + \eta \tag{2b}$$

$$\zeta_1 = \zeta_1^0 + \eta. \tag{2c}$$

Per definition $\zeta_1^0=0°$, and then β_1^0 and γ_1^0 are real physical parameters describing the relative orientations of the cofactors.

For the simulation of the recorded TREPR spectrum, $F(B_0)$, we integrate

$$F(B_0) = \int_0^{2\pi} d\alpha_1 \int_0^{\pi/2} d\alpha_2 \int_0^{2\pi} d\alpha_3 \sin\alpha_2 P(\alpha_2, \alpha_3)$$
$$\times f(B_0, \alpha_1, \alpha_2, \alpha_3), \tag{3}$$

where $f(B_0, \alpha_1, \alpha_2, \alpha_3)$ is the TREPR signal of a particular RC with orientation $(\alpha_1, \alpha_2, \alpha_3)$ as function of B_0. The quantity $f(B_0, \alpha_1, \alpha_2, \alpha_3)$ is calculated using the CCRP model, see Section 3.1. For $\theta=0$ the integration over α_1 can be omitted.

4. Results and discussion

Fig. 3a and b shows the experimental results obtained in the Fabry–Pérot resonators with the two different orientations with respect to the Zeeman field B_0. The dotted lines are the spectra simulations, the bottom lines depict the residua, see below. It is evident that the signal-to-noise ratio for B_0n is better than for $B_0\perp n$. In part, this is because for B_0n neglecting imperfect ordering, only one single orientation is selected, while for $B_0\perp n$ one expects to observe an overlap of all other orientations. This leads to cancellation effects when spectral contributions of different orientations have opposite signs. Furthermore, the spectrum becomes broader. To illustrate the intensity effect, the spectra have been
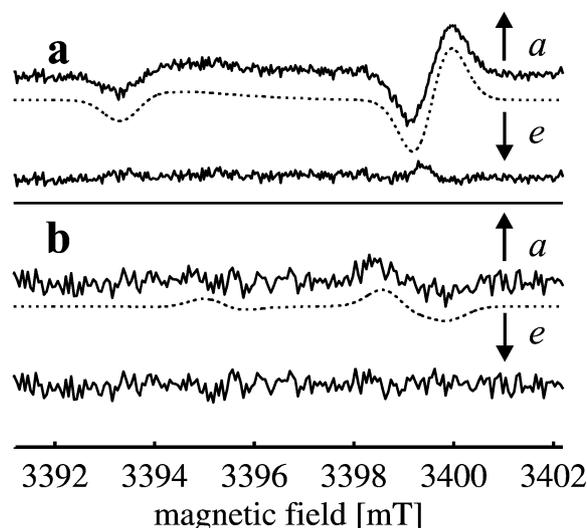

Fig. 3. TREPR spectra of the $P_{700}^{+\cdot}$ $A_1^{-\cdot}$ radical pair in oriented multilayers at 160 K, integrated over the first 800 ns after laser excitation, and spectra simulations (dotted) using the parameters in Table 1. Positive signals correspond to absorption, negative signals to emission of the spin-polarized radical-pair system. The bottom lines depict the respective residua. (a) B_0n, i.e., the magnetic field is perpendicular to the sample mirror. (b) $B_0\perp n$.

vertically scaled according to the intensity ratio expected from the simulations.

For the spectra simulations we have used the parameters collected in Table 1. They are based on previous experiments on disordered samples as well as on single crystals of both protonated and deuterated RCs (see Ref. [11]). As discussed above, for the simulations on 1D oriented multilayers, we need to include three additional parameters, $\varDelta_x$, $\varDelta_y$, and η. Because independent information on these parameters is rare, we have used the recently available high-resolution X-ray structure of PS I [11,14] to discuss these additional parameters on the basis of our experimental results. The best agreement of simulations and experiment could be achieved for an axially symmetric orientation distribution with $\varDelta=\varDelta_x=\varDelta_y=30°$ (Fig. 3). For comparison, the simulations for $\varDelta=20°$ and $40°$ are shown in Fig. 4a and b. $\varDelta=30°$ corresponds to a FWHM of $35°$. An FWHM of $35°$ is similar to what was used for the simulations of X-band ESEEM measurements on $P_{700}^{+\cdot}A_1^{-\cdot}$ of PS I at 0.34 mT X-band EPR (FWHM $30°$) [19] and for simulations of tyrosine radicals, Tyr_D in PS II (FWHM $40°$) [18]. Furthermore, our results give further evidence that the structural parameters published in Ref. [11] fit significantly better than the parameters published before [9,17]. The corresponding molecular structure is illustrated in Fig. 5. However, it should be mentioned that equally good simulations are achievable with the orientation distribution $\varDelta_x=5°$, $\varDelta_y=50°$ and $\eta=-147°$ (simulation not shown), which is nonaxial with respect to C_2. In this case, the simulations are very sensitive to η, which, therefore, could be determined to an accuracy of about $\pm10°$. From the measurements presented it is not possible to decide

Table 1
Parameters used for the simulations in Figs. 3 and 4

D	−0.17 mT		
J_{ex}	10^{-3} mT		
Line width σ	0.7 mT		
$\Delta = \Delta_x = \Delta_y$	30°		
G (P_{700}^+)	2.0030	2.0026	2.0023
G (A_1^-)	2.0062	2.0051	2.0022
Tensor orientations with respect to the membrane			
P_{700}^+ ($\beta_1, \beta_2, \beta_3$)	−165.5	−62.3	−66.2
A_1^- ($\gamma_1, \gamma_2, \gamma_3$)	27.7	−65.2	−12.4
ZFS ($\zeta_1, \zeta_2, \zeta_3$)	0	27.6	–

Except for Δ, the parameters are taken from Ref. [11] (Tables 1 and 4, top line). For the definition of the Euler angles, see Fig. 2. The error of Δ is about ±10°, for the error discussion of the other parameters see Ref. [11].

whether the orientation distribution is axially symmetric or not. However, the fact that the measurements published before could also be well simulated using axially symmetric

orientation distributions [18,19] is an argument in favor of an axially symmetric distribution. In the following, we assume axial symmetry and $\Delta = (30 \pm 10)°$, and we will discuss whether it is possible to increase spectral resolution for structural studies using oriented multilayers.

The aim of TREPR studies on P_{700}^+ A_1^- is to determine relative orientations of P_{700}^+ and A_1^- in their charge separated states, their orientations with respect to the membrane surface, their distance and the orientation of the dipolar axis. Starting from the known structure (Table 1), we have rotated P_{700}^+, A_1^- and the dipolar axis orientation about the respective principal axes, and compared the effect on the spectra simulations both for oriented multilayer (B_0n) and disordered (powder) samples. The changes in the TREPR spectra of multilayers and powders are of comparable magnitude only for rotation of the dipolar axis. For all other rotations, the effect was significantly larger for the
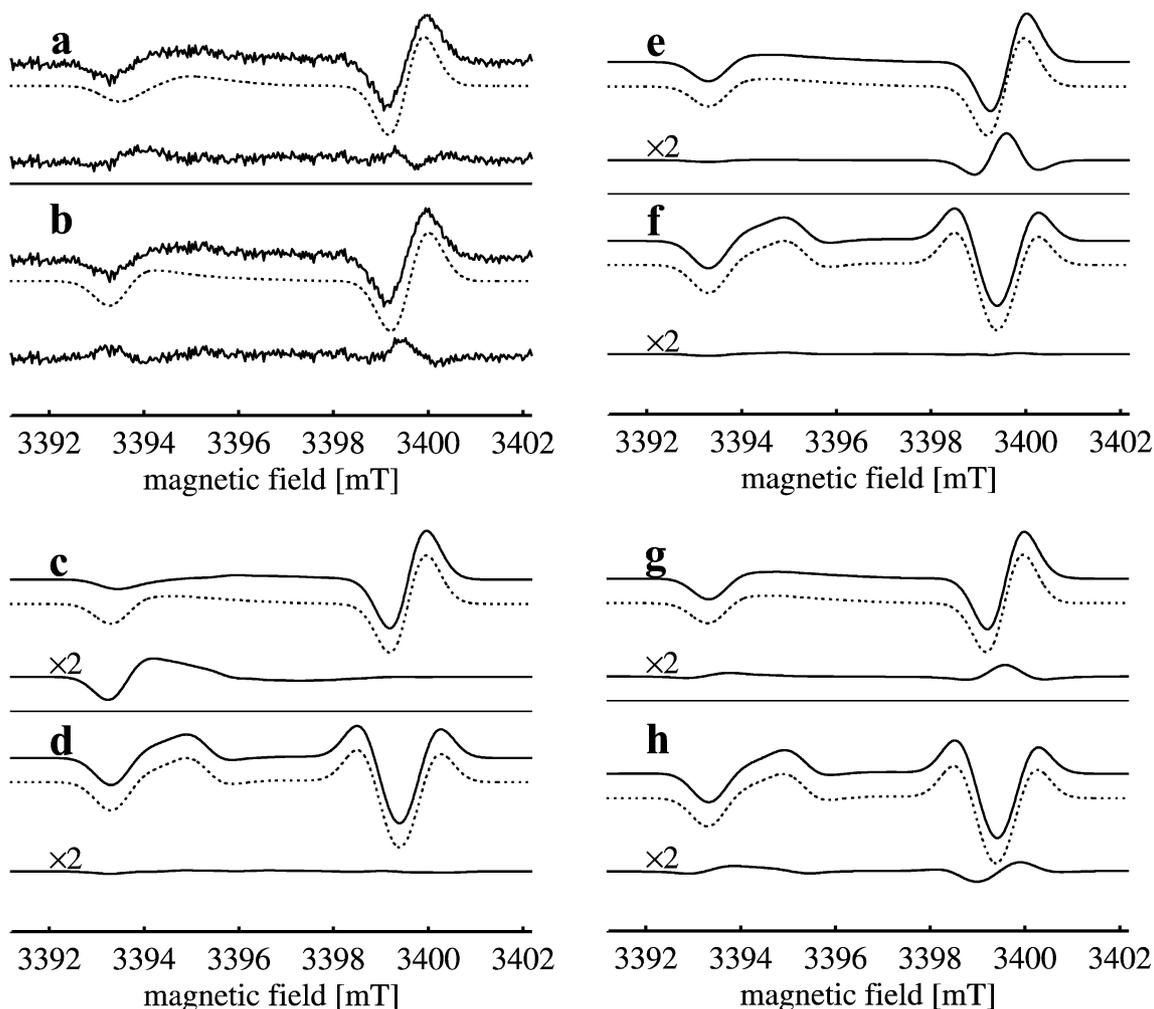

Fig. 4. Effect of different parameters and phase errors on spectra simulations for the orientation B_0n (see Fig. 3a, solid line) and for disordered samples (for experimental results, see Ref. [9]). The other parameters are from Table 1. (a) The dotted line shows the multilayer simulation for the order parameter $\Delta = \Delta_x = \Delta_y = 20°$ (see Eqs. (1a)–(1b)). The solid line shows the experimental result, the bottom line the residuum. (b) Same with $\Delta = \Delta_x = \Delta_y = 40°$. (c) Multilayer simulation assuming that A_1^- is rotated by 10° about its y axis (solid line) compared to simulations without structural changes (dotted line). The residuum is shown below. (d) Same for disordered sample. (e) Multilayer simulation assuming that P_{700}^+ is rotated by 10° about its y axis. (f) Same for disordered sample. (g) Effect of phase error of 5° on the multilayer simulation. (h) Same for disordered sample.
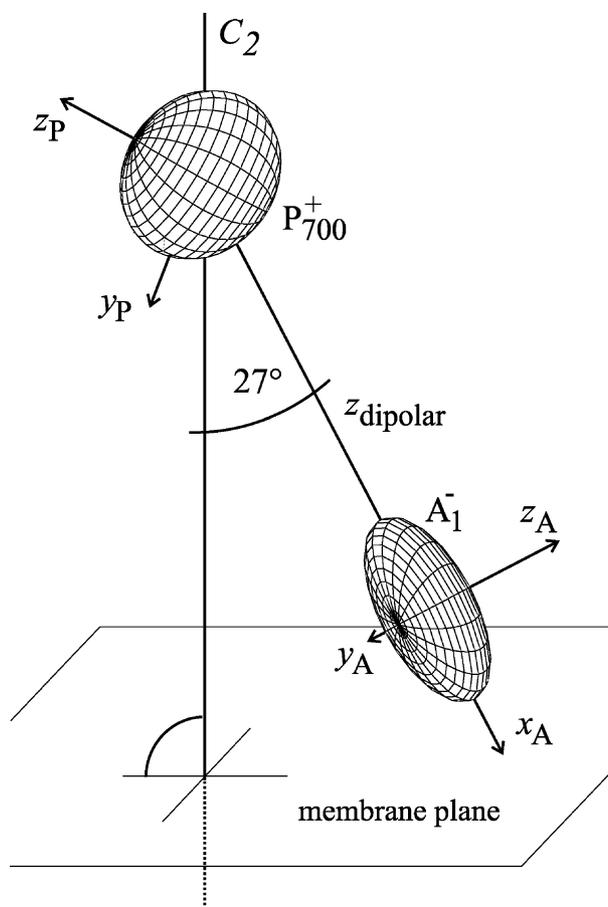
Fig. 5. Illustration of the tensor orientations from Table 1. The lengths of the principal axes of the ellipsoids correspond to the magnitude of the tensor principal values.

multilayers they are still smaller than the effects of structural changes simulated in Fig. 4c–f.

To summarize: Comparing the residua in Figs. 3 and 4, we see that in the case of the PS I RC, much more exact structure determinations can be made with oriented multilayers than with disordered samples. Rotations of A_1 or P_{700} of less than $10°$ already lead to significant changes in the time-resolved radical pair spectra of oriented multilayers. Therefore, this method is interesting for all systems for which one can assume a similar orientation distribution function as for the PS I samples used in our work. A straightforward application would be the study of PS I systems in which the A_1 acceptor is exchanged by non-native quinones [4,23]. These systems show significant change in electron transfer characteristics. Qualitatively, it was concluded from TREPR on disordered samples that the non-native quinones are rotated with respect to the native one [4]. Other possible applications are PS I systems in which the environment of the A_1 acceptor has been changed by site-directed mutagenesis. For example, it has been observed that mutations of W693 slow down the forward electron transfer [22,33]. To investigate structure–function relationship in these systems and to disentangle the influence of various parameters on electron transfer characteristics, it would be very helpful to characterize the orientation of the A_1 in the modified binding pocket using the method presented in this article.

5. Conclusion

Orientation selection in oriented membrane multilayers leads to enhanced resolution of structural parameters in high-field/high-frequency TREPR spectra of radical pairs in RCs. However, the uncertainty of the orientation distribution in multilayers introduces additional ambiguity in the spectra simulation.

For the $P_{700}^+ A_1^-$ radical pair of PS I, which is discussed in this work, structural parameters are already known from other experiments, including EPR. They form the basis of structural models for the cofactors in their charge-separated state.

The TREPR results on $P_{700}^+ A_1^-$ in oriented multilayers were used to evaluate the orientation distribution from the spin-polarized spectra and to discuss the possibilities and limitations of this method, for example for investigating structural changes in mutant photo-systems. Particular emphasis is put on the comparison between effects of structural changes and of experimental errors of orientation distribution and of field and phase calibration. Field and phase calibration is particularly difficult for high-field/high-frequency TREPR. This is because cw spectra of standard reference samples used for the calibration such as Mn^{2+} are normally not recorded simultaneously with the TREPR spectrum. Moreover, different speeds and ranges of magnetic field sweeps of the superconducting magnet for cw and

multilayer spectra. This is illustrated in Fig. 4c–f. They show the effect of a $10°$ rotation of A_1^- (Fig. 4c,d) and P_{700}^+ (Fig. 4e,f) about their y axes, respectively. Apparently, structural changes are much more significant in TREPR spectra of oriented multilayers than in spectra of disordered samples. On the other hand, the change in Fig. 4c is not so different from the changes due to errors of the orientation distribution parameters used (compare Fig. 4a). Furthermore, the change in Fig. 4e is mainly a shift of the effective g value of P_{700}^+ (down-field shift of the right part of the spectrum by approximately 0.1 mT). Therefore, in order to obtain precise structural data, it is necessary to know the orientation-distribution parameter Δ precisely and to have a reliable calibration of the magnetic field axis. Moreover, spectral changes due to structural changes have to be discriminated against phase errors of the TREPR detection. Even with good phase calibration, the phase errors in high-field/high-frequency EPR are about $\pm 5°$, and one observes already contributions of dispersion signals to the line shapes. To illustrate this finding, Fig. 4g and h shows the effect of a $5°$ phase error on multilayer and powder TREPR spectra. Obviously, these effects are not insignificant but, in contrast to disordered samples, for

TREPR would introduce additional errors which have to be carefully minimized. Therefore, in the future, it is planned to record cw EPR spectra simultaneously with TREPR spectra using a Zeeman field modulation of only 0.05 mT. This would allow conventional cw lock-in detection, but is small enough not to distort TREPR line shapes.

To conclude: Based on the determined orientation distribution width of $\Delta=(30\pm10)°$, our spectra simulations show that subtle structural changes in the radical-pair complex in membrane fragments can be more easily detected in oriented multilayer than in disordered samples of PS I in frozen solution. This is particularly promising for future studies on mutant PS I RCs, for which no single crystals are available (see Refs. [20–23]). Apparently, the combination of multifrequency TREPR on disordered samples and on oriented multilayers is a very appealing strategy for structural analysis of transient radical-pair systems in photo-induced electron-transfer processes.

Acknowledgements

References

[1] A.J. Hoff, J. Deisenhofer, Phys. Rep. 287 (1997) 1–248.
[2] D. Stehlik, K. Möbius, Annu. Rev. Phys. Chem. 48 (1997) 745–784.
[3] K. Möbius, Chem. Soc. Rev. 29 (2000) 129–139.
[4] A. van der Est, Biochim. Biophys. Acta 1507 (2001) 212–225.
[5] R. Bittl, S.G. Zech, Biochim. Biophys. Acta 1507 (2001) 194–211.
[6] K. Brettel, Biochim. Biophys. Acta 1318 (1997) 322–373.
[7] K. Brettel, W. Leibl, Biochim. Biophys. Acta 1507 (2001) 100–114.
[8] S. Dzuba, H. Hara, A. Kawamori, M. Iwaki, S. Itoh, Y. Tsvetkov, Chem. Phys. Lett. 264 (1997) 238–244.
[9] A. van der Est, T. Prisner, R. Bittl, P. Fromme, W. Lubitz, K. Möbius, D. Stehlik, J. Phys. Chem., B 101 (1997) 1437–1443.
[10] R. Bittl, S. Zech, J. Phys. Chem., B 101 (1997) 1429–1436.
[11] S.G. Zech, W. Hofbauer, A. Kamlowski, P. Fromme, D. Stehlik, W. Lubitz, R. Bittl, J. Phys. Chem., B 41 (2000) 9728–9739.
[12] O. Klukas, W.-D. Schubert, P. Jordan, N. Krauss, P. Fromme, H.T. Witt, W. Saenger, J. Biol. Chem. 274 (1999) 7351–7360.
[13] O. Klukas, W.-D. Schubert, P. Jordan, N. Krauss, P. Fromme, H.T. Witt, W. Saenger, J. Biol. Chem. 274 (1999) 7361–7368.
[14] P. Jordan, P. Fromme, H. Witt, O. Klukas, W. Saenger, N. Krauss, Nature 411 (2001) 909–917.
[15] P. Fromme, P. Jordan, N. Krauss, Biochim. Biophys. Acta 1507 (2001) 5–31.
[16] A. Rutherford, P. Sétif, Biochim. Biophys. Acta 1019 (1990) 128–132.
[17] F. MacMillan, J. Hanley, L. van der Weerd, M. Knüppling, S. Un, A.W. Rutherford, Biochemistry 36 (1997) 9297–9303.
[18] P. Dorlet, A.W. Rutherford, S. Un, Biochemistry 39 (2000) 7826–7834.
[19] T. Yoshii, H. Hara, A. Kawamori, K. Akabori, M. Iwaki, S. Itoh, Appl. Magn. Reson. 16 (1999) 565–580.
[20] B. Boudreaux, F. MacMillan, C. Teutloff, R. Agalarov, F. Gu, S. Grimaldi, R. Bittl, K. Brettel, K. Redding, J. Biol. Chem. 276 (2001) 37299–37306.
[21] S. Itoh, M. Iwaki, I. Ikegami, Biochim. Biophys. Acta 1507 (2001) 115–138.
[22] S. Purton, D.R. Stevens, I.P. Muhiuddin, M.C.W. Evans, S. Carter, S.E.J. Rigby, P. Heathcote, Biochemistry 40 (2001) 2167–2175.
[23] A. van der Est, S. Brown, P. Ragogna, J. Pushkar, S.G. Zech, D. Stehlik, G.S.P. Chitnis, J. Golbeck, 12th International Congress on Photosynthesis, Brisbane, ISBN 0643 06711 6, CSIRO Publishing (www.publish.csiro.au/PS2001), 2001, contribution S6-005.
[24] T.F. Prisner, M. Rohrer, K. Möbius, Appl. Magn. Reson. 7 (1994) 167–183.
[25] O. Burghaus, M. Rohrer, T. Götzinger, M. Plato, K. Möbius, Meas. Sci. Technol. 3 (1992) 765–774.
[26] M.C. Thurnauer, J.R. Norris, Chem. Phys. Lett. 76 (1980) 557–561.
[27] G.L. Closs, M.D.E. Forbes, J.R. Norris, J. Phys. Chem. 91 (1987) 3592–3599.
[28] D. Stehlik, C.H. Bock, J. Petersen, J. Phys. Chem. 93 (1989) 1612–1619.
[29] P.J. Hore, Analysis of polarized electron paramagnetic resonance spectra, in: A.J. Hoff (Ed.), Advanced EPR, Applications in Biology and Biochemistry, Elsevier, Amsterdam, 1989, pp. 405–440, Chap. 12.
[30] A. Kamlowski, S.G. Zech, P. Fromme, R. Bittl, W. Lubitz, H.T. Witt, D. Stehlik, J. Phys. Chem., B 102 (1998) 8266–8277.
[31] M. Fuhs, G. Elger, A. Osintsev, A. Popov, H. Kurreck, K. Möbius, Mol. Phys. 98 (2000) 1025–1040.
[32] T. Berthold, M. Berthold, U. Heinen, G. Link, O. Poluektov, L. Utschig, J. Tang, M.C. Thurnauer, G. Kothe, J. Phys. Chem., B 103 (1999) 10733–10736.
[33] M. Guergova-Kuras, B. Boudreaux, A. Joliot, K. Redding, PNAS 98 (2001) 4437–4442.